

# TRIS II: search for CMB spectral distortions at 0.60, 0.82 and 2.5 GHz

M. Gervasi<sup>1,2</sup>, M. Zannoni<sup>1</sup>, A. Tartari, G. Boella<sup>2</sup>, and G. Sironi<sup>1</sup>

*Physics Department, University of Milano Bicocca, Piazza della Scienza 3, I20126 Milano  
Italy*

mario.zannoni@mib.infn.it

## ABSTRACT

With the TRIS experiment we have performed absolute measurements of the sky brightness in a sky circle at  $\delta = +42^\circ$  at the frequencies  $\nu = 0.60$ , 0.82 and 2.5 GHz. In this paper we discuss the techniques used to separate the different contributions to the sky emission and give an evaluation of the absolute temperature of the Cosmic Microwave Background. For the black-body temperature of the CMB we get:  $T_{cmb}^{th} = (2.837 \pm 0.129 \pm 0.066)K$  at  $\nu = 0.60$  GHz;  $T_{cmb}^{th} = (2.803 \pm 0.051 \pm_{-0.300}^{+0.430})K$  at  $\nu = 0.82$  GHz;  $T_{cmb}^{th} = (2.516 \pm 0.139 \pm 0.284)K$  at  $\nu = 2.5$  GHz. The first error bar is statistic ( $1\sigma$ ) while the second one is systematic. These results represent a significant improvement with respect to the previous measurements. We have also set new limits to the free-free distortions,  $-6.3 \times 10^{-6} < Y_{ff} < 12.6 \times 10^{-6}$ , and slightly improved the Bose-Einstein upper limit,  $|\mu| < 6 \times 10^{-5}$ , both at 95% confidence level.

*Subject headings:* cosmology: cosmic microwave background, cosmological parameters, observations, diffuse radiation, radio continuum: galaxies

## 1. Introduction

At decimetric wavelenghts the sky brightness temperature ( $T_{sky}$ ) can be written as the sum of different contributions: cosmic microwave background ( $T_{cmb}$ ), galactic emission ( $T_{gal}$ ), unresolved extragalactic radio sources ( $T_{uers}$ ).

---

<sup>1</sup>also Italian National Institute for Astrophysics, INAF, Milano.

<sup>2</sup>also Italian National Institute for Nuclear Physics, INFN, Milano-Bicocca.

The temperature of the cosmic microwave background (CMB),  $T_{cmb}$ , can be considered, for our purposes, as isotropic. The largest anisotropy component is the dipole term  $\Delta T_{dipole}(\alpha, \delta) = T_d \cos \theta$ , with  $T_d = 3.381 \pm 0.007$  mK, and  $\theta$  angle between the direction of observation and the maximum of the dipole at  $(\alpha = 11^h 12^m.2 \pm 0^m.8; \delta = -7^\circ.06 \pm 0^\circ.16)$  ((Bennet et al. 1996); (Fixen et al. 1996) and (Fixen & Mather 2002)). It gives a level of anisotropy well inside the error budget of our absolute measurements. Therefore we will consider in the present paper only the possible dependence of the CMB brightness temperature on the frequency ( $T_{cmb}(\nu)$ ). The frequency dependence could be related to the spectral distortion of the CMB.

The most accurate measurement of the CMB temperature so far made is the one obtained by the COBE-FIRAS team ((Mather et al. 1990); (Mather et al. 1994); (Fixen et al. 1996); (Mather et al. 1999); (Fixen & Mather 2002)). Between 60 to 600 GHz they found a spectrum fully compatible with a black body emitting at the thermodynamic temperature  $T_{cmb}^{th} = 2.725 \pm 0.001$  K (see (Fixen & Mather 2002)). Major spectral distortions in this range are excluded by COBE-FIRAS and the parameters of both the Bose-Einstein and Compton distortions are largely constrained:  $|\mu| < 9 \times 10^{-5}$  and  $|y| < 15 \times 10^{-6}$  (both at 95% CL, see (Fixen et al. 1996)).

Although very accurate the FIRAS result covers only part of the CMB frequency spectrum. In particular it does not cover the low frequency region where TRIS measurements were made and where distortions can be expected. Table 1 collects the measurements of the CMB temperature made at frequencies below few GHz starting from the 80's. At these low frequencies the error bars are much larger than at FIRAS frequencies, essentially because of the large uncertainties associated to the absolute calibration procedures and to the presence of important foregrounds.

To improve the low frequency situation it has been proposed in the past to carry on measurements of the CMB temperature from space: LOBO ((Sironi et al. 1995); (Sironi et al. 1997)) for which TRIS is a pathfinder and DIMES (Kogut 1996). DIMES has been then transformed in a balloon program (ARCADE), whose results have been published recently (see (Kogut et al. 2004); (Fixen et al. 2004); (Singal et al. 2006)).

The black-body spectrum of the CMB is the result of the complete thermalization of the Universe in the pre-recombination era. At that time the strong interactions among the different components of the cosmic plasma were efficient enough to re-establish immediately the thermodynamic equilibrium after an energy injection. Nevertheless small deviations from the black-body distribution can survive if the energy injection occurred at a red-shift  $z \lesssim 10^6$ . In the pre-recombination era ( $z \gtrsim 10^4 - 10^3$ ) a kinetic equilibrium is re-established through the Compton scattering, Double Compton scattering and the Bremsstrahlung mechanism.

The resulting spectrum assumes a typical shape described by the Bose-Einstein or by the Compton distribution. For a review of these mechanisms see (Zeldovich & Sunyaev 1969), (Sunyaev & Zeldovich 1970), (Zeldovich et al. 1972), (Illarionov & Sunyaev 1975a), (Illarionov & Sunyaev 1975b), (Sunyaev & Zeldovich 1980), while detailed calculations have been performed by (Burigana et al. 1991a), (Burigana et al. 1991b), (Burigana et al. 1995) and (Daly 1991). These types of distortions are described by the chemical potential  $\mu$  and the Comptonization parameter  $y$ , whose possible values have been already limited by COBE-FIRAS.

Energy injections after the recombination era are responsible of spectral distortions without any possibility of re-thermalization. Among these processes there is the photon injection through free-free mechanism in a re-ionized universe (see (Bartlett & Stebbins 1991)). This effect depends on the square of the wavelength and therefore is dominant at very low frequencies and is not constrained by the COBE-FIRAS measurements. Other possible distortions are related to the formation of primordial molecules and to the formation of structures at large scale. Both these mechanisms are difficult to be modeled but, at least in the case of the formation of primordial molecules, a not negligible effect could be expected at decimetric wavelengths (see (Varshalovich & Khersonskii 1977) and (Dubrovich & Stolyarov 1995)).

The galactic emission ( $T_{gal}(\nu, \alpha, \delta)$ ) is anisotropic and has a power law frequency spectrum:  $T_{gal}(\nu) = T_{gal}(\nu_0)(\nu/\nu_0)^\beta$ . Its importance and properties are analyzed in the companion paper (Tartari et al. 2008) (hereafter Paper III) from which we take the spectral index  $\beta$  we will use in the following.

The contribution of the unresolved extragalactic radio sources (UERS),  $T_{uers}$ , has also a power law frequency spectrum, but for a low resolution experiment it can be considered isotropic. In the following we will take it from the model developed by (Gervasi et al. 2008) on the basis of the source number counts measurements available in literature.

After a brief summary of TRIS experiment (Section 2), in Section 3 we discuss the techniques used to separate the components of  $T_{sky}$  and the results obtained for  $T_{cmb}$ . The implications of these results in terms of spectral distortions are presented in Section 4.

## 2. TRIS

TRIS experiment, fully described in the companion paper (Zannoni et al. 2008) (hereafter Paper I), is a set of three absolute total power radiometers. They were operated (1996-2000) at Campo Imperatore (Italy), a site at 2000 m a.s.l. where a reasonable compromise of radio-quietness, winter accessibility and heavy logistic was achieved. After a few

tests to minimize the effects of the radio-frequency interferences, the radiometers were tuned at:  $\nu = 0.60050$  GHz,  $\nu = 0.81785$  GHz,  $\nu = 2.42775$  GHz. All the radiometers had the same block diagram (see Figure 1). The antennas, rectangular horns corrugated on the E plane, were geometrically scaled and had the same beam size ( $18^\circ(E) \times 23^\circ(H)$  HPBW) with side-lobes lower than -40 db. Two modes of observations were used: drift scan mode and absolute measurement mode. During the drift scans the receivers were connected to the horn by a room temperature waveguide-to-coaxial transition. During absolute measurements, the radiometers’ front-ends were cooled at liquid helium temperature, as shown in Figure 1.

## 2.1. Drift Scans

Most of the experiment lifetime was used to carry on drift scans of the sky with the antennas aimed at the zenith ( $\delta = +42^\circ$ ). To avoid sun contamination and keep the gain variation under control, the sky profiles were built using only data collected at nighttime, when the temperature stability of the receivers was better than  $\pm 0.1^\circ\text{C}$ . Receiver gain and change of the antenna impedance matching were checked at regular time intervals using the Internal Calibrator (IntCal block in Figure 1), based on a noise source with a stability better than  $\sim 0.1\%$  over months. Data collected in rainy and cloudy conditions were rejected from the analysis (for details see Sections 4.2 and 4.4 of the Paper I).

Once properly combined the TRIS drift scans gives complete profiles of  $T_{sky}$  versus the right ascension  $\alpha$ , along the circle at declination  $\delta = +42^\circ$  at 0.60 and 0.82 GHz. At 2.5 GHz the level of radio frequency interferences hampered the construction of a complete profile. The error budget on the variations of the temperature along the profiles at 0.60 and 0.82 GHz are dominated by the uncertainties on the corrections for drifts and offsets and by the uncertainty in the determination of the temperature scale. In particular, at  $8^h \lesssim \alpha \lesssim 16^h$ , the galactic halo region, which has been observed redundantly, an uncertainty upon temperature variations in the range from 5 to 10 mK was achieved, both at 0.60 GHz and 0.82 GHz. At  $\alpha \sim 20^h$  (see Figure 2), the galactic disk region, the larger uncertainty we obtained is due to the smaller number of drift scans. In drift scan mode of observation (shown in Figure 2) the zero level of the scale of temperature is arbitrary.

## 2.2. Absolute Measurements

During the absolute measurement campaigns the radiometers were equipped with the cryogenic front-end. The horns were attached to stainless steel waveguides and brass waveguide-

to-coaxial transition which were immersed in liquid helium to reduce their thermal emissions. Each cryostat housed also a Single Pole Triple Through (SPTT in Figure 1) passive resonant switch. The SPTT connects, for absolute calibration, the receiver alternately with the antenna or two reference dummy loads: Cold Load (CL) at  $\sim 4$  K and Warm Load (WL) at  $\sim 270$  K. Typical calibration runs, involving cold and warm loads and the internal calibration mark (CM) are shown in Figure 3. The transfer function of all the components between the horn mouth and the switch output (waveguides, transitions, cables, etc.) have been measured in laboratory. The only parts we were unable to measure are the flares of the horns: their attenuation has been calculated. Accurate measurements of the temperature profiles of these components, both inside and outside the cryostat, during the observations, combined with the attenuation, allow to evaluate and subtract their contribution to the receiver output. At 0.82 GHz a failure of the dewar housing the cryogenic front-end during absolute measurements forced us to use an alternative set-up with only the SPTT switch cooled in liquid Helium. This is the reason why the 0.82 GHz values of the Sky Temperature have an higher systematic uncertainty (see for details the Sections 4.2 and 4.3 of the Paper I).

Comparing the signals measured looking at the sky with the signals produced by the warm and cold loads we get absolute values of the antenna temperature at various points along the circle at  $\delta = +42^\circ$ . Subtracting the environmental contribution (ground, atmosphere, RF interferences) we get absolute values of the sky temperature at the same points. Details of this procedure are given in the Paper I (Section 4.3.1), while results are presented in Table 2. The ground contribution has been calculated convolving the antenna beam with a black-body at 290 K having the profile of the horizon at Campo Imperatore. The atmospheric transmission and emission have been evaluated using the model described in (Ajello et al. 1995). The effect of RF interferences have been evaluated by using metal shields around the horns. At 0.60 and 0.82 GHz they were well inside the system noise. At 2.5 GHz they were so frequent and strong that observations were possible only rarely (for details see Paper I).

The Sky Temperature values ( $T_{Sky}$ ) measured during the absolute observations were used to set the zero level of the drift scans. As a matter of fact, the drift scans, once reduced to the top of the atmosphere, had the same dynamic range of the absolute measurements data. In this way we got the absolute Sky Temperature also for those regions of the sky not observed during the absolute measurements. Table 3 reports the final accuracy of the absolute values of  $T_{Sky}$ . The systematic uncertainty on the zero level quoted in Table 3 ( $\Delta T_{zero}$ ) applies also to the drift scan profiles once corrected for the zero level. In Table 3 the number of independent sky positions analyzed during the absolute measurements is also shown.

### 3. Separation of the components of $T_{sky}$

At TRIS frequencies the brightness temperature of the sky can be written as:

$$T_{sky}(\nu, \alpha) = T_{cmb}(\nu) + T_{gal}(\nu, \alpha) + T_{uers}(\nu) \quad (1)$$

The contribution ( $T_{uers}$ ) of unresolved extragalactic radio sources (UERS) at the TRIS frequencies can be obtained from (Gervasi et al. 2008) and immediately subtracted from  $T_{sky}$ . The values we used are summarized in Table 4.

To disentangle  $T_{cmb}$  and  $T_{gal}$  at 0.60 and 0.82 GHz we take advantage of the accurate TRIS profiles of  $T_{sky}$  versus  $\alpha$  (see Section 3.1). At 2.5 GHz, because no drift scan is available, we followed a different approach (see Section 3.2).

#### 3.1. Analysis of the measurements at 0.60 and 0.82 GHz

##### 3.1.1. The position difference technique (PDT)

The separation of the components of  $T_{sky}$  is possible because it is made of an isotropic component ( $T_{cmb}$  and  $T_{uers}$ ) plus an anisotropic component ( $T_{gal}$ ). The profiles of  $T_{sky}$  measured by TRIS at 0.60 and 0.82 GHz give the variation of  $T_{sky}$  with the right ascension  $\alpha$  along a circle at constant declination ( $\delta = +42^\circ$ ). We can take a pair of positions in the sky ( $\alpha_1, \alpha_2$ ) at the two frequencies  $\nu_1 = 0.60$  GHz and  $\nu_2 = 0.82$  GHz, and write a set of linear equations:

$$\begin{aligned} T_{sky}(\nu_1, \alpha_1) - T_{uers}(\nu_1) &= T_{cmb}(\nu_1) + T_{gal}(\nu_1, \alpha_1) \\ T_{sky}(\nu_1, \alpha_2) - T_{uers}(\nu_1) &= T_{cmb}(\nu_1) + T_{gal}(\nu_1, \alpha_2) \\ T_{sky}(\nu_2, \alpha_1) - T_{uers}(\nu_2) &= T_{cmb}(\nu_2) + T_{gal}(\nu_2, \alpha_1) \\ T_{sky}(\nu_2, \alpha_2) - T_{uers}(\nu_2) &= T_{cmb}(\nu_2) + T_{gal}(\nu_2, \alpha_2) \end{aligned} \quad (2)$$

The galactic signal depends both on  $\alpha$  and  $\nu$ , and we can write:

$$T_{gal}(\nu, \alpha) = T_{gal}(\nu_0, \alpha) \left( \frac{\nu}{\nu_0} \right)^{\beta(\alpha, \nu, \nu_0)} \quad (3)$$

In spite of this simple analytical form, also the spectral index  $\beta(\alpha, \nu, \nu_0)$  depends on  $\alpha$  and  $\nu$ . Putting  $\nu_1 = \nu_0$  and taking the difference between pairs of Equations 2 we get:

$$\begin{aligned} T_{sky}(\nu_1, \alpha_1) - T_{sky}(\nu_1, \alpha_2) &= T_{gal}(\nu_1, \alpha_1) - T_{gal}(\nu_1, \alpha_2) \\ T_{sky}(\nu_2, \alpha_1) - T_{sky}(\nu_2, \alpha_2) &= T_{gal}(\nu_1, \alpha_1) m(\alpha_1) - T_{gal}(\nu_1, \alpha_2) m(\alpha_2) \end{aligned} \quad (4)$$

with  $m(\alpha) = (\nu_2/\nu_1)^{\beta(\alpha)}$ . We can use these equations to separate the microwave sky components if we can find two positions  $\alpha_1$  and  $\alpha_2$  such that  $\beta(\alpha_1) \neq \beta(\alpha_2)$  ( $m(\alpha_1) \neq m(\alpha_2)$ ),  $T_{sky}(\nu_1, \alpha_1) \neq T_{sky}(\nu_1, \alpha_2)$  and  $T_{sky}(\nu_2, \alpha_1) \neq T_{sky}(\nu_2, \alpha_2)$ . When these conditions, necessary to break the degeneracy, are satisfied, from Equations 4 follows:

$$\begin{aligned} [T_{sky}(\nu_2, \alpha_1) - T_{sky}(\nu_2, \alpha_2)] - [T_{sky}(\nu_1, \alpha_1) - T_{sky}(\nu_1, \alpha_2)] m(\alpha_1) &= \\ = T_{gal}(\nu_1, \alpha_2) [m(\alpha_1) - m(\alpha_2)] \end{aligned} \quad (5)$$

an equation we can use to extract  $T_{gal}$ , if  $m(\alpha_1)$  and  $m(\alpha_2)$  are known. If  $m$  is unknown we can look for different pair of points close to  $\alpha_1$  and  $\alpha_2$  respectively, write a system of equations and extract  $T_{gal}(\alpha)$  and  $m(\alpha)$ . Finally, going back to Equations 2 we can get a number of values of  $T_{cmb}(\nu)$  in the sky regions around  $\alpha_1$  and  $\alpha_2$ .

### 3.1.2. *TT-plot technique*

For each pair of sky positions  $\alpha_i$  and  $\alpha_j$ , around  $\alpha_1$  and  $\alpha_2$  respectively, we can write:

$$m(\alpha_{i,j}) = \frac{T_{sky}(\nu_2, \alpha_i) - T_{sky}(\nu_2, \alpha_j)}{T_{sky}(\nu_1, \alpha_i) - T_{sky}(\nu_1, \alpha_j)} \quad (6)$$

In principle one can repeat this procedure for all the pair of points along the drift scan profiles at 0.60 and 0.82 GHz obtained by TRIS, look for regions where the conditions to break the degeneracy are satisfied and get  $m$ .

This can be done very efficiently using a well known graphical method, the TT-plot technique, which allows to look for correlation between the sky temperatures at two frequencies  $\nu_1$  and  $\nu_2$ . Introduced by (Turtle et al. 1962) and widely used also recently e.g. in (Davies et al. 1996) and (Platania et al. 1998) to analyze maps of the microwave sky, it allows to find regions where the values of  $m$  (and  $\beta$ ) are well defined. These "homogeneous" regions can be selected by plotting  $T_{sky}(\nu_2, \alpha)$  versus  $T_{sky}(\nu_1, \alpha)$ : all the positions  $\alpha$  inside these regions distribute themselves along a straight line whose slope is  $m$ . This means that in these positions the spectral index can be considered uniform:  $\beta(\alpha_i) \simeq \beta(\alpha_j)$ .

As evident from Equation 6 the values of  $m(\alpha)$  (and  $\beta(\alpha)$ ) obtained depend only on the temperature variations and are not affected by uncertainties on the zero level of the two scales of temperature ( $\Delta T_{zero}$ ). In the Paper III (Tartari et al. 2008), Section 3, the TT-plot method has been applied to the TRIS profiles at 0.60 and 0.82 GHz (shown in Figure 2). It shows that, along the circle at  $\delta = +42^\circ$ , there are two regions where the spectral indices are well defined and different: here the conditions to solve Equation 5 apply. These two regions are:  $9^h \lesssim \alpha_1 \lesssim 11^h$ , the halo region at the highest galactic latitude; and  $20^h \lesssim \alpha_2 \lesssim 21^h$ , the galactic disk, close to the Cygnus region.

### 3.1.3. Monte Carlo analysis

Having the above information we can now solve the equation and get  $T_{cmb}$  and  $T_{gal}$  at various  $\alpha$ . We did it by a Monte Carlo simulation. In this way we take directly into account the effects of the uncertainties, both statistic and systematic, of the measured quantities ( $T_{sky}(\nu, \alpha)$ ) on the evaluation of the unknown quantities. We also assumed as prior the information coming from the TT-plot method used in Paper III: i.e. central value and width of the distribution of the spectral index  $\beta(\alpha)$ . Following this approach we obtained the distribution of the values of  $T_{cmb}(\nu_1)$  and  $T_{cmb}(\nu_2)$ , which include the effect of the distribution of all the parameters involved in the Equations 2. The error bars of  $T_{cmb}$  have been evaluated by using the bootstrap method. The systematic uncertainty of the zero level of  $T_{sky}$  ( $\Delta T_{zero}$  in Table 3), not included in the MC analysis, has been quoted separately.

The values of  $T_{cmb}$  we obtained are distributed around a well defined central value, as shown in Figure 4 and summarized in Table 5. We have also obtained the galactic emission in the halo and in the disk regions (see Table 6). As shown by the system of Equations 4, the absolute temperature of the galaxy, evaluated using this method, is not affected by the systematic uncertainty ( $\Delta T_{zero}$ ) on the zero level of  $T_{sky}$ .

### 3.1.4. Graphic method

In principle graphic methods can be used also to extract  $T_{cmb}$  from a TT-plot. Through each point ( $T_{sky}(\nu_1, \alpha)$ ;  $T_{sky}(\nu_2, \alpha)$ ), at a certain value of  $\alpha$ , of the TT-plot we can draw a straight line of slope  $m(\alpha) = (\nu_2/\nu_1)^{\beta(\alpha)}$  whose intercept  $T_0$  is:

$$T_0 = T_{sky}(\nu_1, \alpha) - T_{sky}(\nu_2, \alpha) \frac{1}{m(\alpha)} \quad (7)$$



After a simple algebra, and assuming  $T_{cmb}(\nu_1) \equiv T_{cmb}(\nu_2) = \overline{T_{cmb}}$ , we get:

$$\overline{T_{cmb}} = \frac{m}{m-1} \left[ T_{sky}(\nu_1) - T_{sky}(\nu_2) \frac{1}{m} - T_{uers}(\nu_1) \left( 1 - \frac{q}{m} \right) \right] \quad (8)$$

with  $q = T_{uers}(\nu_2)/T_{uers}(\nu_1)$ . We have used this method in the same halo and disk regions used before. In this way we got values of  $\overline{T_{cmb}}$  in agreement with the results obtained by the PDT method. However: (i) we can not separate the CMB temperature at the two frequencies and (ii) there is an unfavorable combination of systematics on the zero level assessment at the two frequencies:

$$\Delta T_{zero}^{CMB} = \left| \frac{m}{m-1} \right| \Delta T_{zero}^{SKY}(\nu_1) + \left| \frac{1}{m-1} \right| \Delta T_{zero}^{SKY}(\nu_2) \quad (9)$$

which, applied to TRIS data at  $\nu_1 = 0.60$  and  $\nu_2 = 0.82$  GHz, gives  $m \simeq 0.38 - 0.42$  and  $\Delta T_{zero}^{CMB} = {}^{+0.76}_{-0.54}$  K. In order to avoid these limitations we need to consider differences between pairs of positions in the sky. But in this case the set of equations we get is equivalent to the PDT method described above.

### 3.2. Analysis of the measurements at 2.5 GHz

At 2.5 GHz no profile of  $T_{sky}$  vs  $\alpha$  was available. Therefore we were forced to adopt a more straightforward but less accurate method: evaluating  $T_{gal}$  at  $\nu = 2.5$  GHz from independent measurements, by a model, and subtracting it from  $T_{sky} - T_{uers}$  to get  $T_{cmb}$ . We got  $T_{gal}$  extrapolating data from the map of the diffuse radiation at 1.42 GHz prepared by (Reich & Reich 1986), which is the one in literature closest to  $\nu = 2.5$  GHz, covering the sky region scanned by TRIS. This map has been convolved with the beam of the TRIS antennas in order to get the synthetic drift scan at  $\delta = +42^\circ$ . Then we extrapolated this signal at 2.5 GHz using the spectral index  $\beta$  got from TRIS data at 0.60 and 0.82 GHz (see Paper III). Finally we subtracted  $T_{gal}$  and  $T_{uers}$  from  $T_{sky}$  and got  $T_{cmb}$ . The results are reported in Table 7. Here the statistical uncertainty on the experimental points ( $\Delta T_{stat} = 103$  mK) is larger than at lower frequencies because we have few independent measurements.

### 3.3. Results

The values of  $T_{cmb}$  obtained above, using different methods, are consistent within the error bars (see Section 3.1). This means that the errors (statistics and systematics), proper

of the measurements and arising from the analysis, are well represented by the quoted uncertainty (see Table 5).

The brightness temperatures of the CMB ( $T_{cmb}(\nu)$ ) are converted into thermodynamic black-body temperature ( $T_{cmb}^{th}(\nu)$ ):

$$T_{cmb}^{th}(\nu) = \frac{h\nu}{k \ln(x_b + 1)} \quad (10)$$

where  $x_b = h\nu/kT_{cmb}$ . Results are summarized in Table 8 and in Figure 5 together with the results from previous measurements (see Table 1).

## 4. Discussion

### 4.1. Comparison with the previous measurements

The results obtained by the TRIS experiment represent a significant improvement in the CMB measurements at frequencies lower than 1 GHz.

Above 1 GHz in literature there are more accurate and recent results. These measurements give temperatures of the CMB which, within the error bars, are in agreement with the temperature measured by FIRAS at much higher frequencies. The only exceptions are the results obtained at 1.4 GHz by (Levin et al. 1988) and (Bensadoun et al. 1993). It is hard to fit these results only with the spectral distortions allowed by COBE-FIRAS (see (Fixen et al. 1996)).

Among the more recent experiments, the most promising program is ARCADE (see (Kogut 2003)). At the frequencies  $\nu = 10$  and 30 GHz ARCADE has obtained results with error bars of 10 and 32 mK respectively (see (Fixen et al. 2004)), which at 8.0 and 8.3 GHz go up to 120 and 160 mK respectively (see (Singal et al. 2006)). The lowest frequency scheduled by ARCADE is 3.3 GHz. Unfortunately above 2 – 3 GHz an accuracy of few mK is necessary to detect or furtherly constrain the limits on distortions produced by Comptonization, Bose-Einstein (*BE*), or free-free (*FF*) processes, set by FIRAS. The search for *BE* and *FF* distortions is better done below 2 – 3 GHz. Here in fact larger distortions can be expected.

We can summarize our results in the following way:

(I) At  $\nu = 0.60$  GHz we reduced the error bar by a factor  $\sim 9$ . Before TRIS the error bar was equally distributed between uncertainties on the temperature of the sky and uncertainties on

the level of the galactic and extragalactic foregrounds (see (Sironi et al. 1990)). The better accuracy of TRIS is due to improvement of the experimental set-up and better procedure of foregrounds subtraction.

(II) At  $\nu = 0.82$  GHz the error bar reduction resulting from TRIS is a factor  $\sim 7$ . Due to the failure of the calibrator TRIS results are still dominated by the systematic uncertainty on the zero level, while the error bar due to the foregrounds separation is smaller.

(III) The TRIS measurement at  $\nu = 2.5$  GHz does not improve but is fully compatible with the previous results (see Table 1). Combined with all the observations in literature we get the value  $T_{cmb}^{th}(2.5 \text{ GHz}) = 2.680 \pm 0.110$  K.

## 4.2. The spectral distortions

We can now combine TRIS results with the data in literature and look for better limits on spectral distortions. The Compton distortions are important only in the Wien region of the CMB spectrum. Therefore in the following discussion we will not consider them.

The Bose-Einstein (*BE*) distortion is, conversely, important at frequencies lower than 1 GHz. Various analyses suggest it can produce a dip in the brightness temperature at sub-GHz frequencies (see (Burigana et al. 1995); (Burigana & Salvaterra 2003)). The minimum is expected at a frequency:

$$\nu_{min}^{BE} \propto [\Omega_b h^2]^{2/3} \quad (11)$$

where  $\Omega_b$  is the baryon density and  $h$  is the Hubble constant parameter. Assuming the WMAP results for  $\Omega_b h^2$  (see (Spergel et al. 2007)) we expect  $\nu_{min}^{BE} \sim 0.3 - 0.4$  GHz. Detection of  $\nu_{min}^{BE}$  should give an independent estimate of the baryon density  $\Omega_b$ . The dip amplitude is related to the chemical potential  $\mu$ , by  $\Delta T_{BE} \propto \mu [\Omega_b h^2]^{-2/3}$ . The limit set by COBE-FIRAS on the chemical potential ( $|\mu| < 9 \times 10^{-5}$ ) implies a spectral distortion  $\Delta T_{BE} \lesssim 17$  mK (95% CL), so the current measurements at low frequency, including TRIS, are not yet accurate enough to detect  $\nu_{min}^{BE}$  and constrain furtherly  $\Omega_b$ .

The free-free emission (*FF*) is expected to produce a temperature deviation with a quadratic dependence on the wavelength:

$$\Delta T_{ff} = T_0 \frac{Y_{ff}}{x^2} \quad (12)$$

where  $Y_{ff}$  is the optical depth to free-free emission and  $x$  is the dimensionless frequency (see (Bartlett & Stebbins 1991)). This kind of distortion is expected in case of re-ionization of the intergalactic medium. The amplitude of the cosmological signal depends on the integrated column density of ionized gas produced at the redshift of formation of the first collapsed objects (Kogut 2003) and on the thermal history of the IGM through the electrons' temperature  $T_e(z)$ . The current upper limit set by the previous measurements at low frequency is  $|Y_{ff}| < 1.9 \times 10^{-5}$  (Bersanelli et al. 1994). A lower limit can be set by the observed Lyman- $\alpha$  forest:  $|Y_{ff}| \gtrsim 8 \times 10^{-8}$  and  $\Delta T_{ff} \gtrsim 2 - 3$  mK at  $\nu = 0.6$  GHz (Haiman & Loeb 1997). A distortion  $\Delta T_{ff} \sim 30$  mK at  $\nu = 0.6$  GHz, corresponding to  $|Y_{ff}| \sim 1.3 \times 10^{-6}$  due to a clumpy component from halos has been suggested by (Oh 1999). Moreover several reionization models have been studied by (Weller et al. 1999), where values of  $|Y_{ff}| \sim (0.5 - 4) \times 10^{-8}$  are suggested for different scenarios.

Combining TRIS measurements and the data in literature we get a data set which has been used to fit the distorted ( $FF + BE$ ) spectra of  $T_{cmb}$ . It includes all the measurements reported in the Table 1, plus the COBE-FIRAS data (Fixen et al. 1996) and the measurements made by ARCADE ((Fixen et al. 2004); (Singal et al. 2006)). We have combined the uncertainties of TRIS data assuming for the statistical one ( $\sigma$ ) a normal distribution and for the systematic one ( $\Delta T_{zero}$ ) a uniform distribution. We set new limits to  $FF$  effect:  $-6.3 \times 10^{-6} < Y_{ff} < 12.6 \times 10^{-6}$  at 95% confidence level. We also improved marginally the upper limits to  $BE$  distortions:  $|\mu| < 6 \times 10^{-5}$  at 95% CL. The undistorted black-body temperature has also been fitted and we have confirmed, as expected, the results obtained by (Fixen & Mather 2002). In Figure 6 we show the maximum frequency distortions, due to  $FF$  effect, allowed after the present analysis. As clearly shown in Figure 6, the major improvement in the upper limits of  $Y_{ff}$  is due to the TRIS measurements, in particular the one at 0.60 GHz. The limits on  $Y_{ff}$  cover positive and negative values. The sign depends on the difference between the electron temperature  $T_e$  in the ionized medium and the radiation temperature  $T_\gamma$ . Mechanisms of recombination cooling can in fact lower the electron temperature down to  $T_e \gtrsim 0.2T_\gamma$  corresponding to  $Y_{ff} \gtrsim -2.3 \times 10^{-5}$  (see (Stebbins & Silk 1986)).

### 4.3. Accuracy and perspectives

The total error budget of the CMB temperature measured by TRIS can be roughly separated in two blocks: uncertainty in the absolute measurements ( $\Delta T_{zero}$ ); uncertainty due to the procedure of foregrounds subtraction ( $\sigma$ ). For TRIS data at 0.60 and 0.82 GHz the statistics is not the dominant source of uncertainty. At 2.5 GHz the results are limited also by the statistics.

Systematic uncertainties on the zero level are set by the capability of controlling and measuring losses and temperatures of the front-end components. As discussed in Paper I at 0.60 GHz we get an accuracy  $\Delta T_{zero} = 66$  mK, a value achievable also at 0.82 GHz (we could not reach it due to the failure of the cryogenic system).

The evaluation of the foregrounds and their subtraction from  $T_{sky}$  is the other main source of uncertainty. The UERS brightness temperature can be evaluated by analyzing the number counts measurements available in literature (see (Gervasi et al. 2008)). Improvements on this value can only come from better source count measurements. The galactic emission has been obtained as a byproduct of TRIS observations by the TT plot method. A technique which works properly if the signals are taken by identical instruments at different wavelengths. The use of existing maps is hampered by intercalibration problems, pointing errors, beam shape accuracy, etc. Minor source of uncertainty are the atmospheric and ground contribution to the antenna temperature. These terms can be controlled by a proper design of the experiment.

We estimate that the best accuracy achievable at TRIS frequencies for  $T_{cmb}$ , using the TRIS methods, is  $\Delta T_{tot} \sim 100$  mK. Better results require to cool down the full front-end, including the horn, and use a cryogenic calibrator in front of it. This is the strategy adopted by ARCADE, but this experiment is limited to frequencies  $\nu \gtrsim 3$  GHz (see (Fixen et al. 2004) and (Singal et al. 2006)). Probably multifrequency space experiments at long wavelengths (see for example proposals like LOBO ((Sironi et al. 1995); (Sironi et al. 1997)) and DIMES (Kogut 1996)), taking advantage of the very stable conditions available in space, should allow to bring  $\Delta T_{tot}$  below 100 mK also at frequencies lower than 1 GHz.

## 5. Conclusions

Starting from the absolute measurements of the sky brightness temperature, performed by the TRIS experiment, and presented in Paper I (Zannoni et al. 2008), we have evaluated the absolute temperature of the Cosmic Microwave Background at  $\nu = 0.60, 0.82$  and 2.5 GHz.

The thermodynamic temperatures of the CMB we get are:  $T_{cmb}^{th} = (2.837 \pm 0.129 \pm 0.066)K$  at  $\nu = 0.60$  GHz;  $T_{cmb}^{th} = (2.803 \pm 0.051 \pm_{-0.300}^{+0.430})K$  at  $\nu = 0.82$  GHz;  $T_{cmb}^{th} = (2.516 \pm 0.139 \pm 0.284)K$  at  $\nu = 2.5$  GHz. The first error bar is  $1\sigma$  statistics, while the second one is the systematic on the zero level assessment.

Thanks to improvements of the absolute calibration system and in the foregrounds separation technique TRIS succeeded in reducing previous uncertainties by a factor  $\sim 9$  at

$\nu = 0.60$  GHz and by a factor  $\sim 7$  at  $\nu = 0.82$  GHz. At 2.5 GHz TRIS results are in agreement with the previous measurements.

These results, used to look for CMB spectral distortions, give an upper limit to the chemical potential  $|\mu| < 6 \times 10^{-5}$  (95% CL) used to describe the  $BE$  distortions. We have also constrained the free-free distortions to:  $-6.3 \times 10^{-6} < Y_{ff} < 12.6 \times 10^{-6}$  (95% CL), approaching the values suggested by observations of the Lyman- $\alpha$  forest (Haiman & Loeb 1997).

**Acknowledgements:** The TRIS activity has been supported by MIUR (Italian Ministry of University and Research), CNR (Italian National Council of Research) and the Universities of Milano and of Milano-Bicocca. The logistic support at Campo Imperatore was provided by INFN, the Italian Institute of Nuclear Physics, and its Laboratorio Nazionale del Gran Sasso. The authors acknowledge also an anonymous referee for his comments which helped us to improve the quality of the results presented.

## REFERENCES

- Ajello, C., Bonelli, G., Sironi, G., 1995, ApJS 96, 643
- Bartlett, J.G., and Stebbins, A., 1991, ApJ, **371**, 8-13.
- Bennet, C.L., et al., 1996, ApJ, **464**, L1-L4.
- Bensadoun, M., et al., 1993, ApJ, **409**, 1-13.
- Bersanelli, M., et al., 1994, ApJ, **424**, 517-529.
- Burigana, C., De Zotti, G., and Danese, L., 1991a, ApJ, **379**, 1-5.
- Burigana, C., Danese, L., and De Zotti, G., 1991b, A&A, **246**, 49-58.
- Burigana, C., De Zotti, G., and Danese, L., 1995, A&A, **303**, 323-330.
- Burigana, C., and Salvaterra, R., 2003, MNRAS, **342**, 543-556.
- Daly, R.A., 1991, ApJ, **371**, 14-28.
- Davies, R.D., Watson, R.A. & Gutiérrez, C.M., 1996, MNRAS, 278, 925
- De Amici, G., et al., 1988, ApJ, **329**, 556-566.
- De Amici, G., et al., 1990, ApJ, **359**, 219-227.
- De Amici, G., et al., 1991, ApJ, **381**, 341-347.
- Dubrovich, V.K., and Stolyarov, V.A., 1995, A&A, **302**, 635-638.
- Fixen, D.J., Cheng, E.S., Gales, J.M., Mather, J.C., Shafer, R.A., and Wright, E.L., 1996, ApJ, **473**, 576-587.
- Fixen, D.J., and Mather, J.C., 2002, ApJ, **581**, 817-822.
- Fixen, D.J., et al., 2004, ApJ, **612**, 86-95.
- Gervasi, M., Tartari, A., Zannoni, M., Boella, G., and Sironi, G., 2008, ApJ, in press; *astro-ph/08034138*, 28 March 2008.
- Haiman, Z., and Loeb, A., 1997, ApJ, **483**, 21-37.
- Illarionov, A.F., and Sunyaev, R.A., 1975a, Soviet Ast., **18**, 413-419.
- Illarionov, A.F., and Sunyaev, R.A., 1975b, Soviet Ast., **18**, 691-699.

- Kogut, A., 1996, *astro-ph/9607100*.
- Kogut, A., 2003, *New A Rev.*, **47**, 945-951.
- Kogut, A., et al., 2004, *ApJS*, **154**, 493-499.
- Levin, S.M., et al., 1988, *ApJ*, **334**, 14-21.
- Mandolesi, N., Calzolari, P., Cortiglioni, S., and Morigi, G., 1984, *Phys. Rev. D*, **29**, 2680-2682.
- Mandolesi, N., et al., 1986, *ApJ*, **310**, 561-567.
- Mather, J.C., et al., 1990, *ApJ*, **354**, L37-L40.
- Mather, J.C., et al., 1994, *ApJ*, **420**, 439-444.
- Mather, J.C., Fixen, D.J., Shafer, R.A., Mosier, C., and Wilkinson, D.T., 1999, *ApJ*, **512**, 511-520.
- Oh, S.P., 1999, *ApJ*, **527**, 16-30.
- Platania, P., Bensadoun, M., Bersanelli, M., De Amici, G., Kogut, A., Levin, S., Maino, D. & Smoot, G.F., 1998, *ApJ*, 505, 473
- Raghunathan, A., and Subrahmanyan, R., 2000, *J. Astroph. Astron.*, **21**, 1-17.
- Reich, P., and Reich, A., 1986, *A&AS*, **63**, 205-292.
- Singal, J., et al., 2006, *ApJ*, **653**, 835-842.
- Sironi, G., Inzani, P., and Ferrari, A., 1984, *Phys. Rev. D*, **29**, 2686-2689.
- Sironi, G., and Bonelli, G., 1986, *ApJ*, **311**, 418-424.
- Sironi, G., Limon, M., Marcellino, G., Bonelli, G., Bersanelli, M., Conti, G. and Reif, K., 1990, *ApJ*, **357**, 301-308.
- Sironi, G., Bonelli, G., and Limon, M., 1991, *ApJ*, **378**, 550-556.
- Sironi, G., Bonelli, G., Dall'Oglio, G., Pagana, E., De Angeli, S., and Perelli, M., 1995, *Astrophys. Lett.*, **32**, 31-36.
- Sironi, G., Boella, G., Gervasi, M., Finocchiaro, G., and Attin , P., 1997, *Proc. 48th International Astronautical Congress*, **IAF-97**, q.1.08.



- Spergel, D.N., et al., 2007, ApJS, **170**, 377-408.
- Staggs, S.T., Jarosik, N.C., Wilkinson, D.T., and Wollak, E.J., 1996, ApJ, **458**, 407-418.
- Stebbins, A., and, Silk, J., 1986, ApJ, **300**, 1-19.
- Sunyaev, R.A., and, Zeldovich, YA.B., 1970, Ap&SS, **7**, 20-30.
- Sunyaev, R.A., and, Zeldovich, YA.B., 1970, ARA&A, **18**, 537-560.
- Tartari, A., Zannoni, M., Gervasi, M., Boella, G., and Sironi, G., 2008, ApJ, submitted.
- Turtle, A.J., Pugh, J.F., Kenderdine, S. & Pauliny-Toth, I.I.K., 1962, MNRAS, 124, 297
- Varshalovich, D.A., and Khersonskii, V.K., 1977, Soviet Ast.Lett., **3(4)**, 155-156.
- Weller, J., Battye, R.A., and Albrecht, A., 1999, Phys. Rev. D, **60**, 103520.
- Zannoni, M., Tartari, A., Gervasi, M., De Lucia, A., Passerini A., Cavaliere, F., Boella, G., and Sironi, G., 2008, ApJ, submitted.
- Zeldovich, YA.B., and Sunyaev, R.A., 1969, Ap&SS, **4**, 301-316.
- Zeldovich, YA.B., Illarionov, A.F., and Sunyaev, R.A., 1972, *Soviet Phys. JEPT*, **35**, 643-648.

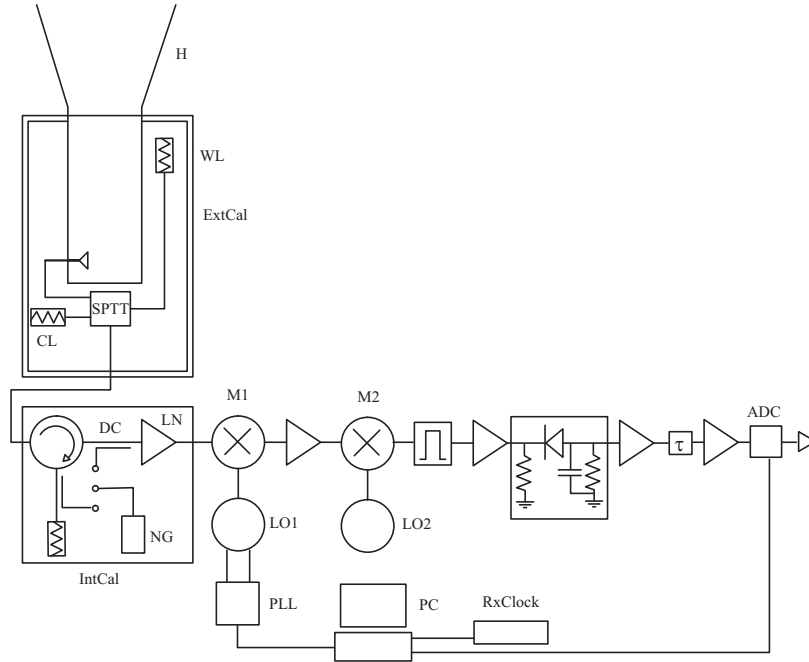


Fig. 1.— Schematic of TRIS antennas and receivers. The set-up of the absolute measurements using the cryogenic front-end is shown. The internal calibrator block (IntCal) is also shown. This schematic is the same at the three frequencies (0.60, 0.82 and 2.5 GHz) of the TRIS experiment.

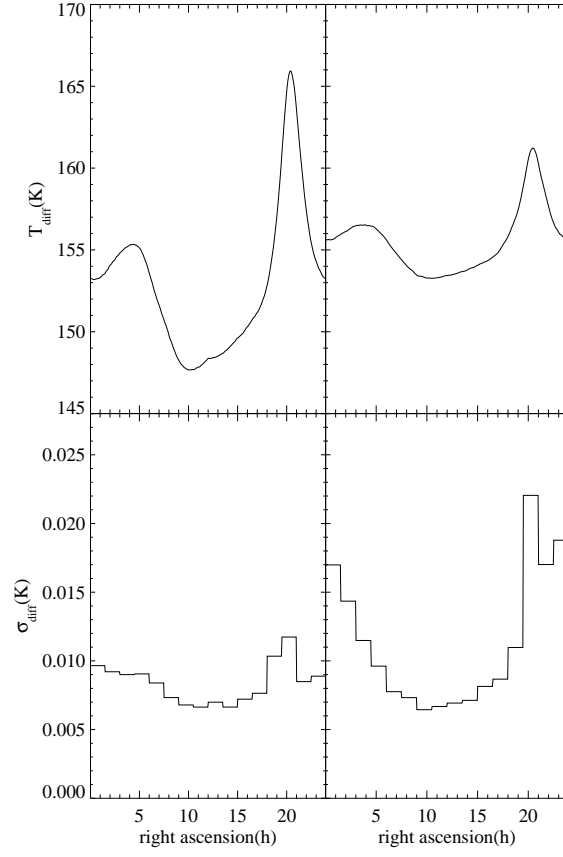


Fig. 2.— Drift scan profiles at 0.60 and 0.82 GHz, with arbitrary zero level. The reported uncertainties represent the statistical error bar, which is the result of the collection of a large number of single drift scan measurements.

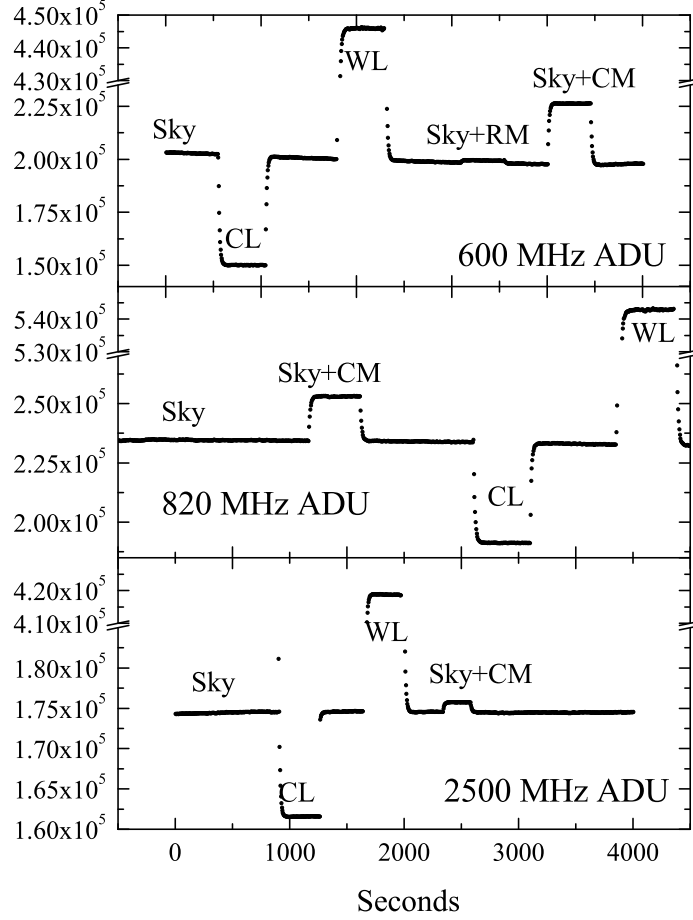


Fig. 3.— A typical run of absolute measurements at the three frequencies of TRIS. We measured the sky (Sky), the Cold Load (CL), the Warm Load (WL), the internal calibration mark (Sky+CM) and the impedance matching (Sky+RM). Signals are still in arbitrary digital units (ADU).

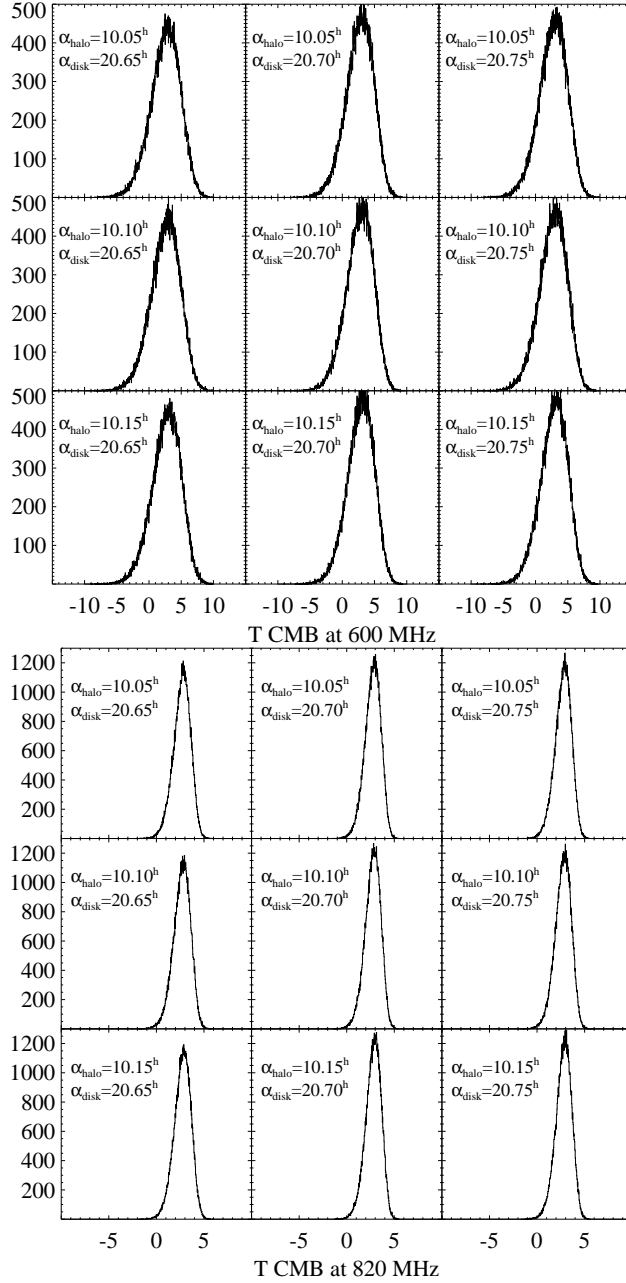


Fig. 4.— Brightness temperature of CMB evaluated with the position difference technique at 0.60 and 0.82 GHz. We got values from 288 pairs of position in the sky (32 positions in the halo  $\times$  9 positions in the disk). Here we show the Monte Carlo realizations in 9 samples of sky position pairs.

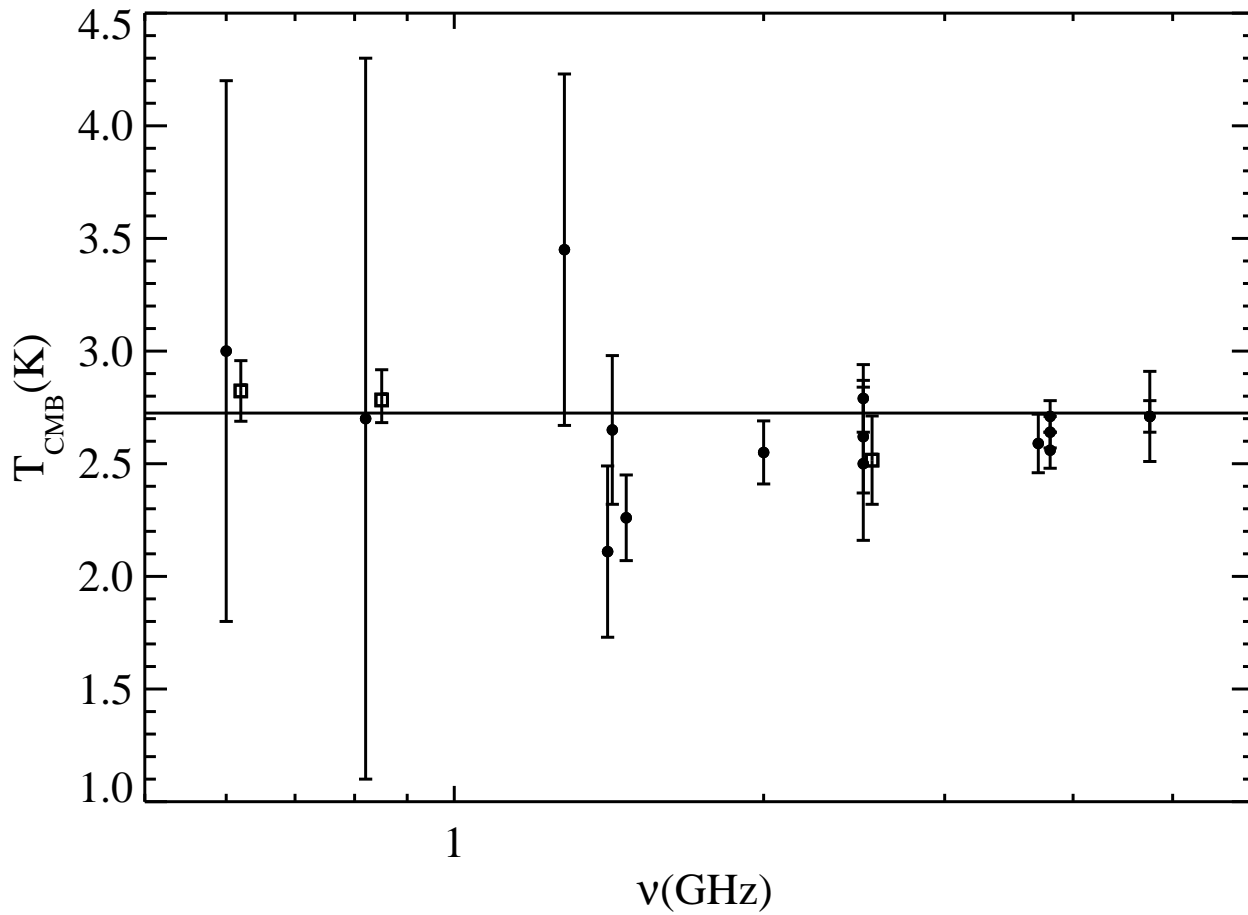


Fig. 5.— The CMB thermodynamic temperature measured at low frequencies (see Table 1). For easier comparison with previous measurements (solid circles), TRIS data points (open squares) have been slightly shifted in frequency. The horizontal solid line is the CMB temperature obtained by FIRAS at higher frequencies.

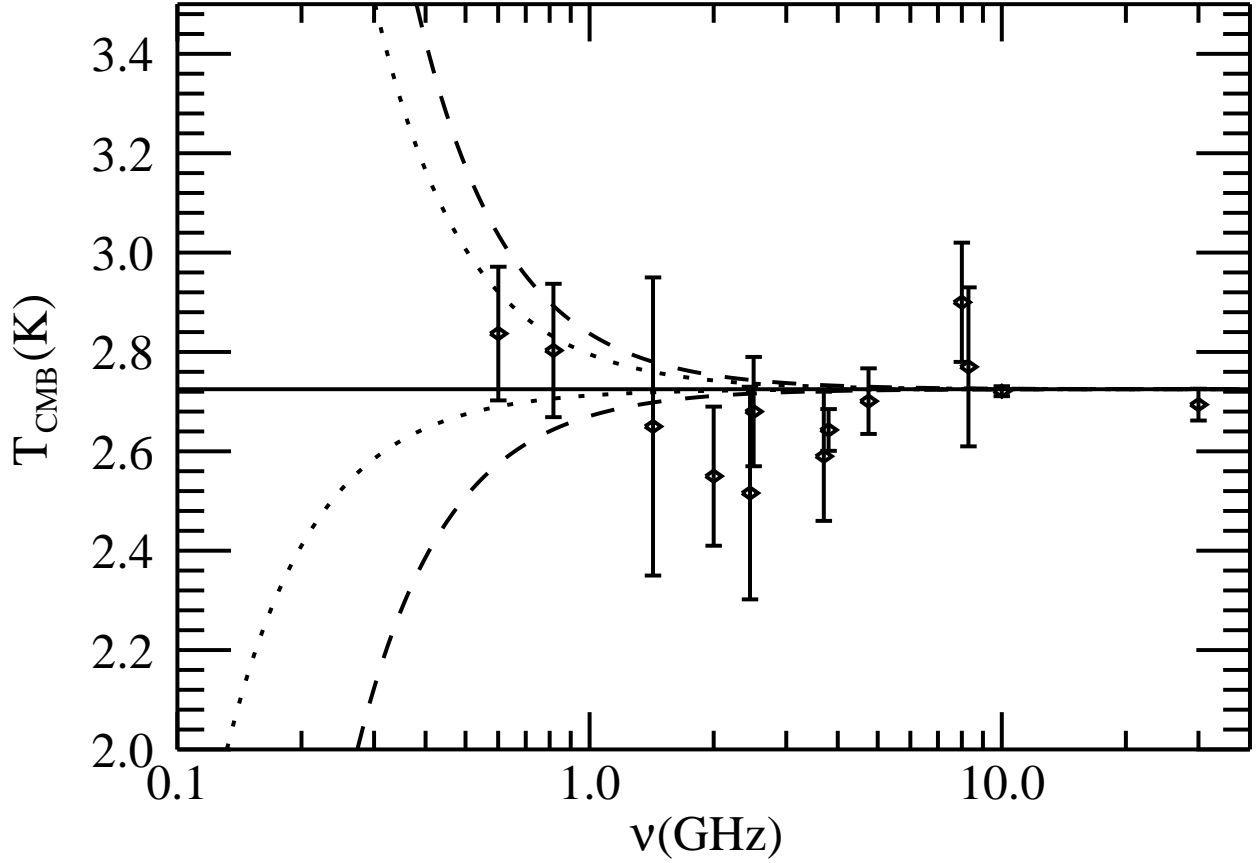


Fig. 6.— Distorted spectra due to  $FF$  effect and measured CMB temperatures. Short dashed lines correspond to  $1\sigma$  upper limits, while long dashed lines correspond to  $2\sigma$  upper limits (95% CL). The solid line is the undistorted CMB temperature. Measurements at the same frequencies have been combined in this plot. Here we report the error bars quoted in literature for the various experiments. TRIS data error bars ( $1\sigma$ ) result from the combination of statistical and systematic uncertainties.

Table 1. A summary of low frequency CMB absolute temperature measurements collected starting from the 80’s.

$\lambda$ (cm)	$\nu$ (GHz)	$T_{cmb}$ (K)	Reference
50.0	0.60	$3.0 \pm 1.2$	(Sironi et al. 1990)
36.6	0.82	$2.7 \pm 1.6$	(Sironi et al. 1991)
23.4	1.28	$3.45 \pm 0.78$	(Raghunathan & Subrahmanyam 2000)
21.3	1.41	$2.11 \pm 0.38$	(Levin et al. 1988)
21.05	1.425	$2.65^{+0.33}_{-0.30}$	(Staggs et al. 1996)
20.4	1.47	$2.26 \pm 0.19$	(Bensadoun et al. 1993)
15.0	2.0	$2.55 \pm 0.14$	(Bersanelli et al. 1994)
12.0	2.5	$2.62 \pm 0.25$	(Sironi et al. 1984)
12.0	2.5	$2.79 \pm 0.15$	(Sironi & Bonelli 1986)
12.0	2.5	$2.50 \pm 0.34$	(Sironi et al. 1991)
8.1	3.7	$2.59 \pm 0.13$	(De Amici et al. 1988)
7.9	3.8	$2.56 \pm 0.08$	(De Amici et al. 1990)
7.9	3.8	$2.71 \pm 0.07$	(De Amici et al. 1990)
7.9	3.8	$2.64 \pm 0.07$	(De Amici et al. 1991)
6.3	4.75	$2.71 \pm 0.20$	(Mandolesi et al. 1984)
6.3	4.75	$2.70 \pm 0.07$	(Mandolesi et al. 1986)

Table 2. Local contribution to the antenna temperature in the TRIS experiment. Atmospheric emission was evaluated by using a model (Ajello et al. 1995); ground contribution was evaluated convolving the ground profile with the antenna side-lobes; RF interferences were directly measured.

$\nu_0$	0.60 GHz	0.82 GHz	2.5 GHz
$T_{atm}$ (K)	$1.088 \pm 0.023$	$1.221 \pm 0.016$	$1.570 \pm 0.025$
$e^{-\tau_{atm}}$	$0.995 \pm 0.001$	$0.995 \pm 0.001$	$0.993 \pm 0.001$
$T_{ground}$ (K)	$0.07^{+0.06}_{-0.03}$	$0.07^{+0.06}_{-0.03}$	$0.07^{+0.06}_{-0.03}$
$T_{rfi}$ (K)	$< 0.01$	$< 0.01$	$9.82 \pm 0.26$



Table 3. Accuracy of the absolute measurements of  $T_{sky}$  performed by TRIS at  $\delta = +42^\circ$ .

$\nu$ (GHz)	$\Delta T_{stat}$ (mK)	$\Delta T_{zero}$ (mK)	# sky positions
0.60	18	66	34
0.82	32	$^{+430}_{-300}$ <sup>†</sup>	12
2.5	10	284	6

<sup>†</sup>The zero level uncertainty at 0.82 GHz coming from the absolute calibration is  $\Delta T_{zero} = 659$  mK. The quoted value comes after astrophysical assumption on the galactic signal (see Paper III (Tartari et al. 2008), Section 3).

Table 4. Contribution of the unresolved extragalactic radio sources to the sky brightness temperature at the frequencies of the TRIS experiment.

$\nu$ (GHz)	$T_{uers}$ (mK)
0.60	$934 \pm 24$
0.82	$408 \pm 10$
2.50	$22 \pm 1$

Table 5. Brightness temperature of CMB at 0.60 and 0.82 GHz evaluated using the PDT method and the spectral index  $\beta$  obtained with the TT-plot technique as prior in the Monte Carlo simulations. The error bar due to the systematics (zero level assessment) is quoted separately from the rest of the uncertainty.

$\nu$ (GHz)	$T_{cmb}(K)$	$\Delta T_{zero}(K)$	$\Delta T_{MC}(K)$
0.60	2.823	0.066	0.129
0.82	2.783	$^{+0.430}_{-0.300}$	0.051

Table 6. Brightness temperature of the galaxy around the minimum and the maximum, respectively, as measured by TRIS antennas at  $\delta = +42^\circ$ . In the last column the related spectral index is reported.

R A	0.60 GHz	0.82 GHz	
h	$T_{gal}^{TRIS}(K)$	$T_{gal}^{TRIS}(K)$	$\beta$
10.0 (Halo)	$5.72 \pm 0.07$	$2.21 \pm 0.03$	$3.09 \pm 0.15$
20.4 (Disk)	$24.44 \pm 0.07$	$10.38 \pm 0.03$	$2.76 \pm 0.10$

Table 7. Brightness temperature of CMB at 2.5 GHz. The error budget due to the different contributions is quoted separately. Due to the small number of independent measurements, the statistical uncertainty of the experimental points is not negligible.

$\nu$ (GHz)	$T_{cmb}(K)$	$\Delta T_{zero}(K)$	$\Delta T_{stat}(K)$	$\Delta T_{gal}(K)$	$\Delta T_{uers}(K)$
2.50	2.458	0.284	0.103	0.093	0.001

Table 8. Thermodynamic temperature of CMB at 0.60, 0.82 and 2.5 GHz. Systematic and combined statistic ( $1\sigma$ ) error bar are quoted separately.

$\nu$ (GHz)	$T_{cmb}^{th}(K)$	$\Delta T_{zero}(K)$	$\sigma(K)$
0.60	2.837	0.066	0.129
0.82	2.803	$^{+0.430}_{-0.300}$	0.051
2.50	2.516	0.284	0.139